Eur. J. Mineral.
2016, **28**, 581–591
Published online 5 May 2016

Paper presented at the
8th European Conference on Mineralogy and Spectroscopy,
Rome, September 9–11, 2015

Bosiite, $NaFe^{3+}_3(Al_4Mg_2)(Si_6O_{18})(BO_3)_3(OH)_3O$, a new ferric member of the tourmaline supergroup from the Darasun gold deposit, Transbaikalia, Russia

ANDREAS ERTL[1,2,*], IVAN A. BAKSHEEV[3], GERALD GIESTER[2], CHRISTIAN L. LENGAUER[2], VSEVOLOD Yu. PROKOFIEV[3,4] and LIDIYA D. ZORINA[5]

[1] Mineralogisch-Petrographische Abt., Naturhistorisches Museum, Burgring 7, 1010, Vienna, Austria
[2] Institut für Mineralogie und Kristallographie, Geozentrum, Universität Wien, Althanstrasse 14, 1090, Vienna, Austria
*Corresponding author, e-mail: andreas.ertl@a1.net
[3] Geology Department, Lomonosov Moscow State University, Leninskie Gory, Moscow, 119991, Russia
[4] Institute of Geology of Ore Deposits, Petrography, Mineralogy, and Geochemistry, Russian Academy of Sciences, Staromonetny per. 35, Moscow, 119017, Russia
[5] Vinogradov Institute of Geochemistry, Siberian Branch, Russian Academy of Sciences, ul. Favorskogo 1a, Irkutsk, 664033, Russia

Abstract: Bosiite, $NaFe^{3+}_3(Al_4Mg_2)(Si_6O_{18})(BO_3)_3(OH)_3O$, is a new mineral species of the tourmaline supergroup from the Darasun gold deposit (Darasun mine), Vershino-Darasunskiy, Transbaikal Krai, Eastern-Siberian Region, Russia (52°20'24"N, 115°29'23"E). Bosiite formed as a hydrothermal phase in a gold-bearing quartz-vein spatially related to the Amudzhikan–Sretensky subvolcanic K-rich granodiorite-porphyry intrusion. Ores of this deposit are enriched in sulfides (up to 60%). Bosiite is intimately associated with other tourmalines. The first tourmaline generation is bosiite, which is followed by a second generation of oxy-dravite and a third generation of dravite. Bosiite also coexists with quartz and pyrite; further associated minerals in the vein are gangue minerals (quartz, calcite, and dolomite), sulfides (pyrite, arsenopyrite, chalcopyrite, pyrrhotite, tetrahedrite, sphalerite, and galena) and native gold. Crystals of bosiite are dark brown to black with a pale-brown streak. Bosiite is brittle and has a Mohs hardness of 7; it is non-fluorescent, has no observable parting and cleavage. It has a measured density of 3.23(3) g/cm^3 (by pycnometry) and a calculated density of 3.26(1) g/cm^3. In plane-polarized light, it is pleochroic, O = yellow-brown, E = red-brown. Bosiite is uniaxial negative, $\omega = 1.760(5)$, $\epsilon = 1.687(5)$. The mineral is trigonal, space group $R3m$, $a = 16.101(3)$, $c = 7.327(2)$ Å, $V = 1645.0(6)$ Å^3. The eight strongest X-ray diffraction lines in the (calculated) powder pattern [d in Å(I)hkl] are: 2.606(100)(50-1), 8.051(58)(100), 3.008(58)(3-1-2), 4.025(57)(4-20), 3.543(50)(10-2), 4.279(46)(3-11), 2.068(45)(6-1-2), 4.648(28)(300). Analysis by a combination of electron microprobe (EMPA), inductively coupled plasma mass spectrometry (ICP-MS), Mössbauer spectroscopic data and crystal-structure refinement results in the empirical structural formula:

$$^{X}(Na_{0.73}Ca_{0.23}\square_{0.04})_{\Sigma 1.00}\,^{Y}(Fe^{3+}_{1.47}Mg_{0.80}Fe^{2+}_{0.59}Al_{0.13}Ti^{4+}_{0.01})_{\Sigma 3.00}\,^{Z}(Al_{3.23}Fe^{3+}_{1.88}Mg_{0.89})_{\Sigma 6.00}$$
$$^{T}(Si_{5.92}Al_{0.08}O_{18})_{\Sigma 6.00}(BO_3)_3\,^{V}(OH)_3\,^{W}[O_{0.85}(OH)_{0.15}]_{\Sigma 1.00}$$

According to the IMA-CNMNC guidelines, the dominant valence at the Y site is 3+ and the dominant cation is Fe^{3+}. To accommodate the disorder and allocating cations to the Z and Y sites, the recommended procedure leads to the optimized empirical formula (based on 31 O): $^{X}(Na_{0.73}Ca_{0.23}\square_{0.04})$ $^{Y}(Fe^{3+}_{2.40}Fe^{2+}_{0.59}Ti^{4+}_{0.01})^{Z}(Al_{3.36}Mg_{1.69}Fe^{3+}_{0.95})$ $^{T}(Si_{5.92}Al_{0.08}O_{18})$ $(BO_3)_3$ $^{V}(OH)_3\,^{W}[O_{0.85}(OH)_{0.15}]$. Bosiite, ideally $NaFe^{3+}_3(Al_4Mg_2)(Si_6O_{18})(BO_3)_3(OH)_3O$, is related to end-member povondraite, ideally $NaFe^{3+}_3(Fe^{3+}_4Mg_2)(Si_6O_{18})(BO_3)_3(OH)_3O$, by the substitution $^{Z}Al_4 \rightarrow {}^{Z}Fe^{3+}_4$. Further, bosiite is related to oxy-dravite, ideally $Na(Al_2Mg)(Al_5Mg)(Si_6O_{18})(BO_3)_3(OH)_3O$, by the substitutions $^{[6]}Fe^{3+}_3 \rightarrow {}^{[6]}Al_3$.

Bosiite is named after Dr. Ferdinando Bosi, researcher at the University of Rome La Sapienza, Italy, and an expert on the crystallography and mineralogy of the tourmaline-supergroup minerals and the spinels.

Key-words: bosiite; new mineral; tourmaline supergroup; Darasun gold deposit; type locality; Transbaikal Krai; Vershino-Darasunskiy; Russia; crystal structure; chemical composition.

1. Introduction and previous work

The general chemical formula of the tourmaline-supergroup minerals can be written $XY_3Z_6[T_6O_{18}]$ $(BO_3)_3V_3W$, as proposed by Henry *et al.* (2011). These authors and Hawthorne (1996, 2002) suggest occupancies by the following most common cations:

DOI: 10.1127/ejm/2016/0028-2540
0935-1221/16/0028-2540 $ 4.95

$X = \mathrm{Na, K, Ca, \square(vacancy)}$

$Y = \mathrm{Mg, Fe^{2+}, Mn^{2+}, Al, Li, Fe^{3+}, Cr^{3+}, V^{3+}}$

$Z = \mathrm{Al, Mg, Fe^{3+}, V^{3+}, Cr^{3+}}$

$T = \mathrm{Si, Al, B}$

$V = \mathrm{OH, O}$

$W = \mathrm{OH, F, O.}$

Crystal-chemical relations in the tourmaline supergroup and the crystal chemistry of tourmaline-supergroup minerals have been investigated by many authors in the last 40 years (*e.g.*, Povondra & Čech, 1976; Foit & Rosenberg, 1979; Deer *et al*., 1986; Foit, 1989; Hawthorne *et al*., 1993; Hawthorne, 1996, 2002; Henry & Dutrow, 1996; Ertl *et al*., 1997, 2012a, Bosi & Lucchesi, 2004, 2007; Bosi *et al*., 2004, 2005, 2013, 2014; Hughes *et al*., 2004, 2011; Henry *et al*., 2011; Ertl & Tillmanns, 2012; Reznitskii *et al*., 2014; 2015, 2016). Substitutions at the *Y* site are more constrained by size than by valence and hence the variety of cations is larger than at the *Z* site, where substitutions are more constrained by valence than by size (Grice & Ercit, 1993).

Tourmaline, rich in Fe^{3+}, has been recorded from many different localities: from the type locality of povondraite (Žáček *et al.*, 1998), from the cap rock of a salt dome in the Gulf of Mexico (Henry *et al*., 1999), and from evaporite formations in Namibia (Henry *et al*., 2008). Tourmalines from the Larderello geothermal field, Italy (Cavaretta & Puxeddu, 1990), from northern Scandinavia, and from porphyry-copper deposits formed during hydrothermal processes (Baksheev *et al*., 2011). The origin of Al-poor tourmaline from the Western Carpathians is still not clear (Bačík *et al*., 2008). Tourmaline from the Darasun gold deposit is, except for the Mg content, similar to tourmaline formed in evaporites and similar to tourmaline from the Western Carpathians, which are also enriched in Ca, but have a different compositional evolution: from Fe^{3+}-rich tourmaline (bosiite) to Fe-bearing dravite in Darasun, whereas in the Western Carpathians it evolved from schorl–dravite to povondraite. Samples from Darasun are very similar in composition to those from the Vetka porphyry-copper deposit, Chukotka, Russia, and also in Mg and Ca contents (Baksheev *et al*., 2010, 2011). The maximum Fe_{tot} content of tourmaline from Darasun (~5 apfu) is higher than in tourmalines from deposits in porphyry-copper deposits (~3 apfu) (Lynch & Ortega, 1997). In addition, the Fe^{3+}/Fe_{tot} value in tourmalines from the Darasun gold deposit is significantly higher. Tourmaline from porphyry tin deposits also displays a homovalent $AlFe_{-1}$ substitution, but is characterized by a lower Fe^{3+}/Fe_{tot} value (Baksheev *et al*., 2010, 2011, 2012). The latter authors concluded that the homovalent $Fe^{3+} \rightarrow$ Al substitution in tourmaline (also observed in tourmalines from Darasun gold deposit) may be used as prospecting guide for porphyry-style deposits and that tourmalines from Cu, Sn and Au porphyry-type deposits can be distinguished from each other on the basis of Li concentration and the ratio Fe^{3+}/Fe_{tot}.

2. Occurrence, geological and petrological setting

The Darasun gold deposit (Darasun mine), Vershino-Darasunskiy, Transbaikal Krai, Eastern-Siberian Region, Russia (52°20'24"N, 115°29'23"E), was the second mine in terms of gold reserves of the Transbaikal Krai. This deposit is hosted in basic and intermediate igneous rocks. The most ancient rock is metamorphosed Early Palaeozoic gabbro, which was intruded by Middle Palaeozoic and Middle Mesozoic granodiorite, diorite, granite, granosyenite and syenite, and also by granitic rocks of the Amanansky complex of Early Jurassic age. The formation of gold deposits in Transbaikalia seems to be controlled by small intermediate and felsic subvolcanic intrusions enriched in alkalis, which belong to the Middle to Late Jurassic Amudzhikan–Sretensky complex and comprise granite and granodiorite porphyry, fracture-related intrusions and stocks, quartz diorite porphyry, granophyre, felsite and pitchstone dykes (Baksheev *et al*., 2011). The Darasun deposit comprises extensive steeply dipping gold-bearing quartz veins and mineralized zones spatially related to the Amudzhikan–Sretensky subvolcanic K-rich granodiorite porphyry intrusion. Ores of this deposit are rich in sulfides (up to 60%). Gangue minerals are quartz, tourmaline, calcite and dolomite.

Bosiite was found in a sulfide- and gold-bearing quartz vein. Native gold, calcite, dolomite, arsenopyrite, chalcopyrite, pyrrhotite, tetrahedrite, sphalerite and galena occur in the same vein. Bosiite coexists with quartz and pyrite (Fig. 1 and Fig. S1 in Supplementary Material, linked to this article and freely available online at the GSW website of the journal: http://eurjmin.geoscienceworld.org/) and is intimately associated with other tourmalines (Figs 2 and 3). The first tourmaline generation is bosiite, which is followed by a second generation (Fig. 4) of a new tourmaline (recently described as oxy-dravite by Bosi & Skogby,

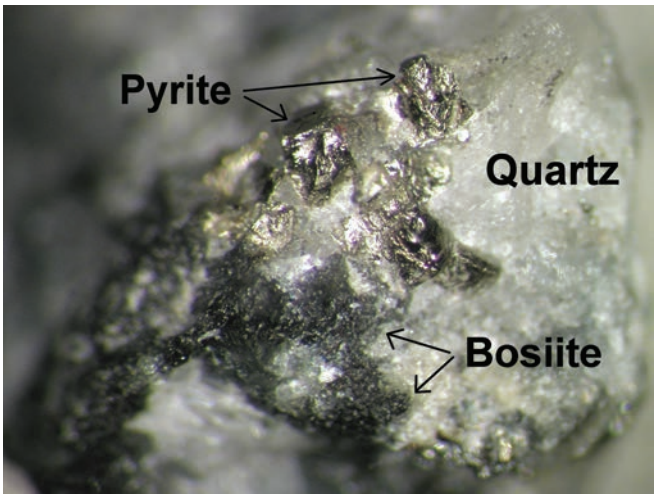

Fig. 1. Black bosiite aggregates (type material), consisting of many tiny crystals, in quartz with pyrite from the Darasun gold deposit (field of view ~3 × 4 mm^2). (online version in colour)

Fig. 2. Photograph of bosiite and oxy-dravite from the Darasun gold deposit (field of view ~3×4 mm^2). (online version in colour)

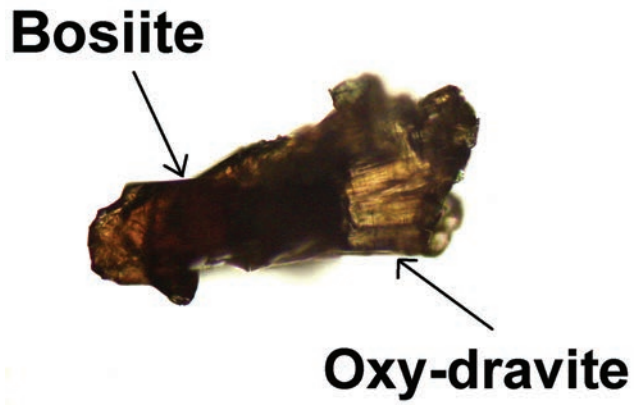

Fig. 3. Photomicrograph (transmitted light) of a crystal aggregate (~300 μm in length) consisting of bosiite and (pale brown) oxy-dravite, from the Darasun gold deposit. (online version in colour)

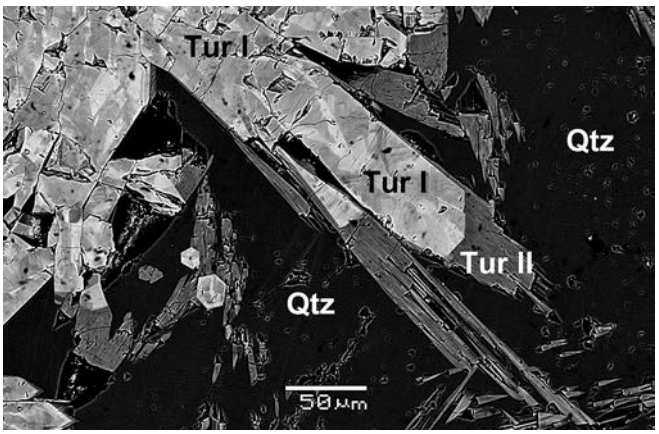

Fig. 4. Back-scattered electron (BSE) image of bosiite (Tur I) and oxy-dravite (Tur II) in quartz (Qtz) from the Darasun gold deposit.

2013), and a third generation, which is represented by dravite (~20 μm thick veins). Depletion of Fe in the second and third generations is caused by deposition of early sulfides.

Baksheev *et al*. (2011) have studied 73 primary fluid inclusions in quartz associated with tourmaline from the bosiite type locality. At room temperature, they found vapour-dominant and aqueous inclusions, indicating boiling in the fluid. Microthermometry indicated that vapour-dominant inclusions homogenize at ~360–380°C and contain a fluid with a salinity of about 1.7 wt% equiv. NaCl. Aqueous inclusions homogenize to liquid at ~350–390°C and contain fluid with a salinity ranging from ~7 to 10 wt% equiv. NaCl. The calculated pressure from vapour-dominated inclusions is 180–230 bars, which corresponds to a depth of 600–800 m. These authors concluded that the fluid inclusions in the associated quartz indicate that first-stage tourmaline (bosiite) precipitated from boiling fluid at low pressure. Boiling favoured the increasing oxygen activity (causing the loss of H_2 into the vapour phase), and resulted in the increase of Fe^{3+} in that tourmaline. Based on these data, bosiite crystallized probably during a hydrothermal event at *PT* conditions of ~0.02 GPa/380°C.

3. Type material

The holotype specimen of bosiite (crystal used for the structural study and coarse-grained sample) is deposited in the collection of the Naturhistorisches Museum Wien, Vienna, Austria, under the catalogue number N 9793. Parts of the cotype material (coarse-grained sample) have also been deposited in the collection of the Fersman Mineralogical Museum, Moscow, Russia (catalogue no. 94999).

4. Experimental details

4.1. Crystal-structure refinement

A fragment of bosiite was separated from the same hand specimen from which the chemistry had been determined; it was subsequently studied on a Bruker AXS Kappa APEXII single-crystal diffractometer equipped with a charge-coupled device (CCD) area detector and an Incoatec Microfocus Source IμS (30 W, multilayer mirror, Mo*K*α). Single-crystal X-ray diffraction data were collected at room temperature (up to 80° 2θ), integrated and corrected for Lorentz and polarization factors with an absorption correction by evaluation of partial multiscans. The structure was refined with SHELXL97 (Sheldrick, 1998) using scattering factors for neutral atoms and a tourmaline starting model from Ertl *et al*. (2010). The H atom bonded to the O3 atom was located from a difference-Fourier map and subsequently refined. Refinement

was done with anisotropic displacement parameters for all non-H atoms. Table 1 provides crystal data and details of the structure refinement. Site occupancies were refined according to well-known characteristics of the tourmaline structure (Na and Ca were refined at the *X* site, Fe and Al were refined at the *Y* and *Z* sites; for other details, see Table 2). The refinement converged at a *R*1(*F*) value of ~3.8% (Table 1). Atom parameters and equivalent isotropic-displacement parameters are given in Table 2, selected interatomic distances in Table 3.

Table 1. Crystal and refinement data of bosiite from the Darasun gold deposit.

a (Å)	16.101(3)
c (Å)	7.327(2)
V (Å^3)	1645.0(6)
Crystal dimensions (mm^3)	0.08 × 0.06 × 0.05
Reflections used for determination of unit-cell parameters	2921
$2\theta_{max}$ (°)	79.96
h, k, l ranges	−29/27, −28/29, −13/12
Number of frames	656
Scan time/frame (s)	200
Total reflections measured	20158
Unique reflections	2286
$R1^*(F)$, $wR2^{\dagger}(F^2)$, $R_{int}^{\ddagger}$ (%)	3.77, 6.27, 7.99
Flack *x* parameter	−0.009(20)
'Observed' refls. [$F_o > 4\sigma(F_o)$]	1766
Extinct. coefficient	0.00077(20)
No. of refined parameters	95
Goodness-of-Fit§	1.026
$\Delta\sigma_{min}$, $\Delta\sigma_{max}$ (e/Å^3)	−0.80, 1.03

Note: X-ray radiation: Mo*K*α (λ = 0.71073 Å); *Z* = 3; space group *R*3*m* (no. 160); multi-scan absorption correction; refinement on F^2. Several sets of phi- and omega-scans with 2° scanwidth/frame were measured up to 80° 2θ (full sphere) at room temperature at crystal-detector distances of 35 mm. Scan mode: sets of ϖ and θ scans.
$^*R1 = \Sigma||F_o| - |F_c||/\Sigma|F_o|$.
$^{\dagger}wR2 = \{\Sigma[w(F_o^2 - F_c^2)^2]/\Sigma[w(F_o^2)^2]\}^{1/2}$.
$w = 1/[\sigma^2(F_o^2) + (aP)^2 + bP]$, $P = [2F_c^2 + \mathrm{Max}(F_o^2, 0)]/3$.
$^{\ddagger}R_{int} = \Sigma|F_o^2 - F_o^2(\mathrm{mean})|/\Sigma[F_o^2]$.
$^{\S}\mathrm{GooF} = S = \{\Sigma[w(F_o^2 - F_c^2)^2]/(n-p)\}^{1/2}$.

4.2. Chemical analysis

A tourmaline fragment was prepared as a section (polished on one side of the sample) for chemical analysis. Concentrations of all elements except B, Li, Be and H were determined with a JEOL JSM–6480LV electron microscope equipped with an Inca Energy–350 energy-dispersion system (EDS) (Laboratory of Analytical Techniques of High Spatial Resolution, Department of Petrology, Lomonosov Moscow State University, Moscow, Russia). Chemical analyses were done by a combination of EDS Inca Energy–350 and WD (wavelength-dispersion) Inca Wave–500 (accelerating potential 15 kV, 64 ± 0.1nA, ~5 μm beam diameter). The concentration of F (MgF_2 was used as a standard) was measured with a WD TAP crystal and the content of the other elements with EDS. For the EDS analyses, line profiles of characteristic X-ray radiation were optimized and normalized using natural silicates as standards (Jarosewich *et al*., 1980). The error for elements with a concentration of ≥5 wt% does not exceed 1.5 relative %.

The Li content was determined by ICP–MS (Institute of Geology of Ore Deposits, Petrography, Mineralogy and Geochemistry (IGEM), Russian Academy of Sciences, Moscow, Russia). Initially, a sample was decomposed with H_2SO_4 and HF in a MILESTONE microwave device according to a four-step program. After the solution was evaporated, treatment by water and dissolution in HNO_3 followed. The measurements were made by using a PLASMA QUAD mass spectrometer (VG Instruments Company).

The crystal-chemical formula was calculated on the basis of 31 (OH, O, F) atoms. The B_2O_3 content was calculated to fill the B site completely. Because of the small amount of available sample, H_2O was not analysed, but was calculated for a charge-balanced formula assuming that there are no vacancies at the *Y*, *Z*, and *T* sites. Analytical data are given in Table 4. Back-scattered

Table 2. Table of positional parameters and their estimated standard deviations for bosiite from the Darasun gold deposit.

Site	*x*	*y*	*z*	U_{eq}	Occupancy
X	0	0	0.7558(3)	0.0229(9)	$Na_{0.75(2)}Ca_{0.25}$
Y	0.87676(4)	1/2*x*	0.34813(7)	0.0108(2)	$Fe_{0.670(6)}Al_{0.330}$
Z	0.70173(4)	0.73795(3)	0.37433(6)	0.0082(1)	$Al_{0.692(4)}Fe_{0.308}$
B	0.89026(14)	2*x*	0.5329(5)	0.0055(7)	$B_{1.00}$
T	0.80939(4)	0.81099(4)	0.98661(8)	0.0090(1)	$Si_{1.00}$
H3	0.736(3)	1/2*x*	0.596(6)	0.026(12)	$H_{1.00}$
O1	0	0	0.2109(6)	0.0157(8)	$O_{1.00}$
O2	0.93905(8)	2*x*	0.5044(3)	0.0139(5)	$O_{1.00}$
O3	0.73689(18)	1/2*x*	0.4749(3)	0.0154(5)	$O_{1.00}$
O4	0.90812(9)	2*x*	0.9168(3)	0.0147(5)	$O_{1.00}$
O5	0.81785(17)	1/2*x*	0.8985(3)	0.0136(4)	$O_{1.00}$
O6	0.80553(12)	0.81430(12)	0.2051(2)	0.0124(3)	$O_{1.00}$
O7	0.71712(11)	0.71736(11)	0.9079(2)	0.0134(3)	$O_{1.00}$
O8	0.79184(11)	0.73116(12)	0.5451(2)	0.0148(3)	$O_{1.00}$

Note: for definition of U_{eq} see Fischer & Tillmanns (1988).

Table 3. Selected interatomic distances (Å) in bosiite from the Darasun gold deposit.

X–O2 (×3)	2.506(3)	*Y*–O1	1.991(2)
–O5 (×3)	2.747(3)	–O6 (×2)	2.028(2)
–O4 (×3)	2.821(3)	–O2 (×2)	2.058(2)
<*X*–O>	2.691	–O3	2.160(3)
		<*Y*–O>	2.054
Z–O8	1.9347(17)	*T*–O6	1.6040(17)
–O6	1.9460(17)	–O7	1.6040(16)
–O7	1.9482(17)	–O4	1.6312(10)
–O8’	1.9600(18)	–O5	1.6454(11)
–O7’	2.0021(17)	<*T*–O>	1.621
–O3	2.0220(12)		
<*Z*–O>	1.969		
B–O8 (×2)	1.375(3)		
–O2	1.376(5)		
<B–O>	1.375		

Table 4. Composition of bosiite from the Darasun gold deposit, Eastern-Siberian Region, Russia (mean of ten electron-microprobe analyses, with standard deviation in parenthesis).

Constituent	Wt.%
SiO_2	33.4 (6)
TiO_2	0.05(4)
Al_2O_3	16.6(7)
B_2O_3*	9.82
FeO_{total}	26.4 (9)
FeO**	3.97
Fe_2O_3**	24.98
MgO	6.4 (6)
CaO	1.21(17)
Na_2O	2.12(13)
K_2O	0.01(1)
H_2O***	2.67
Total	101.27
Constituent	apfu
O basis	31
Si	5.92
$^{[4]}$Al	0.08
Sum *T* site	6.00
$^{[3]}$B	3.00
Ti^{4+}	0.01
Al	3.38
Fe^{2+}	0.59
Fe^{3+}	3.33
Mg	1.69
Sum *Y* + *Z* site	9.00
Ca	0.23
Na	0.73
□	0.04
Sum *X* site	1.00
Sum cations	18.96
OH	3.15

Note: Li (3.1 ppm) was determined on a bulk sample by ICP-MS (Baksheev *et al*., 2011). Fluor, Mn, and Zn are below detection limit. *B_2O_3 is calculated by stoichiometry (see text for details). **The proportion of Fe^{3+} is calculated on the basis of a Mössbauer spectroscopic investigation on a bulk sample (Table 5). ***H_2O was calculated for a charge balanced formula assuming that there are no vacancies at the *Y*, *Z*, and *T* site (see text for details).

electron images were obtained at an accelerating potential of 15 kV and a current intensity of ~15 nA.

4.3. Mössbauer spectroscopy

Approximately 5 mg of tourmaline, consisting mainly of bosiite, were gently crushed under acetone, then mixed with a sugar–acetone solution designed to form sugar coatings around each grain and prevent preferred orientation. The ^{57}Fe spectrum was acquired at 295 K using a SM–2201 Mössbauer spectrometer operating in constant acceleration mode with a ^{57}Co (in Cr) source (Institute of Mineralogy, Ural Division, Russian Academy of Sciences, Miass, Russia). Calibration was done with a standard sample of sodium nitroprusside. Isomer shift refers to an α-Fe absorber at 293 K. Results of the measurements were processed by a least-squares procedure using the SPECTR program in fitting a thin absorber (using a Lorentzian line-shape).

Peak areas were not corrected for differential recoil-free fractions for Fe^{2+} and Fe^{3+} because the appropriate correction factors do not exist.

5. Results

5.1. Optical properties and infrared spectroscopy

In plane-polarized transmitted light, bosiite is pleochroic, *O* = yellow-brown, *E* = red-brown. Bosiite is uniaxial negative, ω = 1.760(5), ϵ = 1.687(5). An infrared spectrum of a first-generation tourmaline single crystal (bosiite) was recorded by Baksheev *et al*. (2011, their Fig. 3B). These authors concluded that the spectrum indicates that a part of Fe^{3+} occurs at the *Z* site. The interactions of three OH groups at the *V* sites with one *Y*-site cation and two *Z*-site cations are indicated by a band in the range 3580–3480 cm^{-1}, with a complex asymmetric profile. In the single-crystal absorption spectrum of bosiite, this band is located at a lower frequency with a maximum at 3552 cm^{-1}. The interaction of the hydroxyl groups at the *W* site with three *Y*-site cations is represented by a single weak band at 3733 cm^{-1} (Baksheev *et al*., 2011).

5.2. Physical properties

Bosiite is brittle and has a Mohs hardness of 7; it is non-fluorescent, has no observable parting and cleavage, and has a vitreous lustre. The megascopic colour of bosiite is black and the streak is dark brown. It has a measured density of 3.23(3) g/cm^3 (by pycnometry) and a calculated density of 3.26(1) g/cm^3 from the empirical formula. The fracture is irregular to uneven and sub-conchoidal. It has a prismatic habit and only unspecified prismatic forms are developed. Twinning

was not observed. The *c*:*a* ratio calculated from the refined unit-cell parameters is 0.455.

5.3. Mössbauer spectrum

The Mössbauer spectrum of bosiite (Fig. 5 in Baksheev *et al*., 2011) was fitted to three doublets (Table 5) that were assigned according to Fuchs *et al*. (1998); Béziat *et al*. (1999) and Dyar *et al*. (1998). The first two doublets ($^{[Y1]}Fe^{2+}$, $^{[Y2]}Fe^{2+}$) are subcomponents of a distribution corresponding to Fe^{2+} at the *Y* site and cover a total area of about 15%. This is also in agreement with the findings of Andreozzi *et al*. (2008), who modelled Fe^{2+} at the *Y* site in tourmalines of the elbaite–schorl–dravite series by three doublets (ΔE_Q = 2.45, 2.19, and 1.72 mm/s). The third strongest doublet, with an isomer shift of 0.57 mm/s, is about 85%, implying that most of the iron in the tourmaline sample examined occurs as Fe^{3+} in octahedral coordination (Baksheev *et al*., 2011). However, the real amount of Fe^{3+} can be higher or lower because of the chemical heterogeneity of the studied sample, of the significant overlap of the peaks in the spectrum and of the additional uncertainty introduced in assuming the same recoil-free fraction for Fe^{2+} and Fe^{3+}. As was shown in previous studies (*e.g*., Dyar *et al*., 1998; Andreozzi *et al*., 2008), the assignment of Fe^{3+} to *Y* or *Z* sites on the basis of Mössbauer data alone is problematic and sometimes not possible. Because of the limited resolution of our Mössbauer data (Table 5), we are not able to use it to establish whether Fe^{3+} occupies both the *Y* and *Z* sites. It is possible that the two expected Fe^{3+} doublets are hidden in a single doublet.

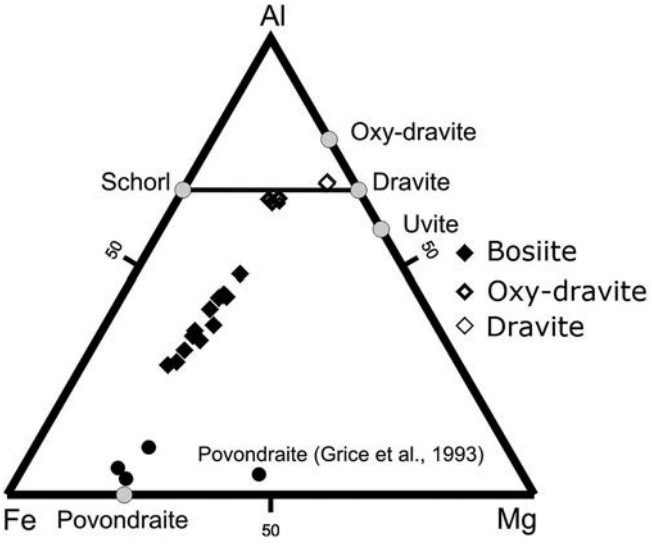

Fig. 5. Compositional variations of tourmalines from the bosiite type locality, Darasun gold deposit. Compositions of bosiite (first tourmaline generation) and of the second (oxy-dravite) and the third (dravite) generations are projected on the Fe–Al–Mg plane (modified from Baksheev *et al*., 2011).

Table 5. Mössbauer parameters for tourmaline from the Darasun gold deposit (bulk sample mainly consisting of bosiite).

$^{[Y1]}Fe^{2+}$	δ, mm/s	1.09
	Δ, mm/s	2.45
	Γ, mm/s	0.32
	% Area	6.8
$^{[Y2]}Fe^{2+}$	δ, mm/s	1.06
	Δ, mm/s	2.21
	Γ, mm/s	0.30
	% Area	7.9
$^{[6]}Fe^{3+}$	δ, mm/s	0.57
	Δ, mm/s	0.67
	Γ, mm/s	0.55
	% Area	85.3
	Total Fe^{3+}	85.3

Notes: Results are given in mm/s relative to the centre point of a Fe-foil calibration spectrum.
δ = isomer shift, Δ = quadrupole splitting, Γ = the width of the peaks at half-maximum.

5.4. Crystal chemistry and structure analysis

The site populations at the *Y* and *Z* sites have been calculated assuming that Fe^{2+} and the small amount of Ti^{4+} occupy the *Y* site, using the method of Wright *et al*. (2000), although we cannot exclude that small amounts of Fe^{2+} and/or Ti^{4+} also occupy the *Z* site (*e.g*., Bosi, 2008; Ertl *et al*., 2012b). The amounts of Al, Fe^{3+} and Mg over the *Y* and *Z* site were optimized (Wright *et al*., 2000) according to mean atomic number and bond valences. Chemical characterization based on electron-microprobe analysis, ICP-MS, single-crystal structure refinement and Mössbauer spectroscopy resulted in the empirical structural formula:

$$\begin{aligned}
&{}^{X}(Na_{0.73}Ca_{0.23}\square_{0.04})_{\Sigma 1.00}\\
&{}^{Y}\left(Fe^{3+}{}_{1.47}Mg_{0.80}Fe^{2+}{}_{0.59}Al_{0.13}Ti^{4+}{}_{0.01}\right)_{\Sigma 3.00}\\
&{}^{Z}\left(Al_{3.23}Fe^{3+}{}_{1.88}Mg_{0.89}\right)_{\Sigma 6.00}\\
&{}^{T}(Si_{5.92}Al_{0.08}O_{18})_{\Sigma 6.00}(BO_3)_3{}^{V}(OH)_3\\
&{}^{W}\left[O_{0.85}(OH)_{0.15}\right]_{\Sigma 1.00}.
\end{aligned} \quad (1)$$

Bosiite is trigonal, with space group *R*3*m*, *a* = 16.101 (3), *c* = 7.327(2) Å, *V* = 1645.0(6) Å^3, *Z* = 3. The eight strongest X-ray diffraction lines in the (calculated) powder pattern [*d* in Å (*I*)*hkl*] are: 2.606(100)(50 - 1), 8.051(58)(100), 3.008(58)(3-1-2), 4.025(57)(4 - 20), 3.543(50)(10 - 2), 4.279(46)(3 - 11), 2.068(45)(6-1-2), 4.648(28)(300) (Table 6). The powder pattern had to be calculated because only a very small amount of bosiite was available, and it was intimately intergrown with oxy-dravite. The Flack parameter of the single-crystal structure shows that no racemic twinning is present (Table 1).

Table 6. X-ray powder diffraction pattern (calculated) for bosiite.

d_{calc} (Å)	I_{calc}	h	k	l
8.051	**58**	**1**	**0**	**0**
5.051	**21**	**2**	**0**	**−1**
4.648	**28**	**3**	**0**	**0**
4.279	**46**	**3**	**−1**	**1**
4.025	**57**	**4**	**−2**	**0**
3.543	**50**	**1**	**0**	**−2**
3.420	8	4	−1	−1
3.243	1	2	0	2
3.148	4	4	0	1
3.043	7	5	−1	0
3.008	**58**	**3**	**−1**	**−2**
2.932	9	5	−2	1
2.660	6	4	−1	2
2.606	**100**	**5**	**0**	**−1**
2.525	2	4	0	−2
2.480	6	6	−2	−1
2.442	6	0	0	3
2.410	18	5	−2	−2
2.370	14	6	−1	1
2.324	5	6	0	0
2.233	1	7	−2	0
2.219	17	5	0	2
2.188	7	7	−3	1
2.162	6	3	0	−3
2.162	8	3	0	3
2.139	6	6	−2	2
2.088	9	4	−2	3
2.068	**45**	**6**	**−1**	**−2**
2.042	8	7	−1	−1
2.013	3	8	−4	0
1.943	**24**	**7**	**−3**	**−1**
1.922	3	8	−3	−1
1.905	7	5	−1	−3
1.870	6	8	−2	1
1.847	1	8	−1	0
1.839	1	7	−1	2
1.806	4	6	−3	3
1.772	2	2	0	−4
1.757	1	9	−3	0
1.750	1	7	0	−2
1.735	2	9	−4	1
1.710	3	8	−2	−2
1.684	6	6	0	3
1.684	17	6	0	−3
1.659	12	9	−2	−1
1.622	4	4	0	4
1.610	15	10	−5	0
1.605	5	9	−4	−2
1.593	2	9	−1	1
1.590	2	5	−2	4
1.563	4	10	−4	−1
1.549	5	9	0	0
1.545	5	9	−2	2
1.534	2	10	−3	1
1.531	15	5	0	−4
1.521	4	10	−2	0
1.504	5	6	−2	−4
1.491	1	9	−1	−2
1.479	15	6	−1	4
1.473	3	8	−1	3
1.473	1	8	−1	−3
1.466	5	10	−4	2
1.457	4	1	0	−5
1.446	5	11	−4	0
1.434	8	11	−5	1
1.434	2	10	−1	1
1.431	10	7	−3	4
1.426	4	9	−3	3
1.426	2	9	−3	−3
1.390	2	11	−3	−1
1.370	9	10	0	1
1.358	4	11	−5	−2
1.351	2	4	0	−5
1.350	1	11	−2	1
1.348	3	7	0	4
1.348	1	8	−3	−4
1.344	5	10	−5	3
1.342	4	12	−6	0
1.332	2	5	−2	5
1.330	1	8	−2	4
1.324	9	11	−1	0
1.321	3	11	−3	2
1.314	2	12	−5	−1
1.308	1	9	0	3
1.303	1	10	0	−2
1.297	10	5	0	5
1.297	1	12	−4	1
1.291	3	10	−2	−3
1.289	3	12	−3	0
1.279	3	9	−4	4
1.255	1	12	−5	2
1.249	3	11	0	−1
1.244	1	11	−4	−3
1.244	1	11	−4	3
1.240	2	12	−4	−2
1.235	2	7	−3	−5
1.234	1	12	−2	−1
1.221	2	0	0	6
1.207	1	7	−1	5

Notes: Only reflections with $I_{calc} \geq 1$ are listed. The eight strongest reflections are in bold.

5.5. *X*-site occupancy

The *X* site in bosiite is occupied mainly by Na (0.73 apfu), but contains also significant amounts of Ca (0.23 apfu) (Table 4). The content of K is at the detection limit (Table 4). The refinement is in excellent agreement with the chemistry ($Na_{0.75(2)}Ca_{0.25(2)}$; Table 2).

5.6. *Y*- and *Z*-site occupancy

The *Y* site is occupied by Fe^{3+} (~1.5 apfu), Mg (~0.8 apfu), Fe^{2+} (~0.6 apfu) and Al (~0.1 apfu). Small amounts of Ti^{4+} (0.01 apfu) might also occupy this site. Only traces of Li occupy the *Y* site (Li content is ~3 ppm; Table 4). The *Y*-site occupancy is consistent with the refinement results (Table 7) and is also in good agreement with the relatively large <*Y*–O> distance of 2.054 Å (Table 3).

The *Z* site is mainly occupied by Al (~3.2 apfu), but contains also significant amounts of Fe^{3+} (~1.9 apfu) and Mg (~0.9 apfu). The *Z*-site occupancy is consistent with the refinement results (Table 7) and is also in good agreement with the enlarged <*Z*–O> distance of 1.969 Å (Table 3). Hawthorne (1996) noted that the occurrence of Al^{3+} at the *Y* site and Mg^{2+} at the *Z* site is due to disorder rather than differences in chemical composition, and that the order–disorder reaction can be expressed as $^{Y}Mg + {}^{Z}Al \leftrightarrow {}^{Y}Al + {}^{Z}Mg$ [$^{Y}Mg^{Z}Al(^{Y}Al^{Z}Mg)_{-1}$]. This disorder is driven by the short-range requirements of O^{2-} at the *W* site (=O1 site) that is associated with 2Al + Mg configurations at the coordinating *Y* sites so as to satisfy its bond-valence requirements (Hawthorne, 1996, 2002). Taylor *et al*. (1995) showed that disorder of Al and Mg over the *Y* and *Z* sites in a calcic tourmaline occurs in tandem with significant O^{2-} at the *W* site. Also in bosiite, the *W* site is mainly occupied by O^{2-} (Table 4). All tourmalines from the type locality of bosiite have an Mg content of ~2 apfu, the *W* site is dominated by O^{2-}, and chemical variations are in accord with the $FeAl_{-1}$ or $AlOFe_{-1}OH_{-1}$ exchange vector (or both). In the suite, the composition of bosiite is substantially deficient in Al (<6 apfu), consistent with a predominance of the $FeAl_{-1}$ exchange (see also Baksheev *et al*., 2011).

5.7. *T*-site occupancy

The *T* site in bosiite is mainly occupied by Si and contains relatively small amounts of Al (~0.1 apfu), consistent with the slightly enlarged <*T*–O> distance of 1.621 Å (Table 3) and data given by MacDonald & Hawthorne (1995) on the Si ↔ Al substitution in tourmaline. There are no indications for significant amounts of $^{[4]}B$ (the <*T*–O> distance is not reduced). Also the amount of ^{Y}Al is too small (~0.1 apfu) for significant amounts of $^{[4]}B$ to occur through short-range order (Fig. 1 in Ertl *et al*., 2008).

5.8. *V*- and *W*-site occupancy

An H atom (H3) at the site associated with O3 was easily located in the refinement. Ertl *et al*. (2002) showed that the bond-angle distortion (σ_{oct}^2) of the ZO_6 octahedron in a tourmaline is largely a function of the <*Y*–O> distance in that tourmaline, although the occupant of the O(3) site (*V* site in the general formula) also affects that distortion. The correlation coefficient, *r*, of <*Y*–O> and σ_{oct}^2 of the ZO_6 octahedron is −0.99 (Fig. 2 in Ertl *et al*., 2005) for all investigated tourmalines whose *V* site is occupied by 3 (OH) groups. Bosiite (with $^{Z}\sigma_{oct}^2$ = 42.47 and <*Y*–O> 2.054 Å; Table 3) lies exactly on the *V* site = 3 (OH) line. Hence, the *V* site of bosiite is completely occupied by $(OH)_3$. No H associated with the O(1) site (*W* site) was found by refinement. Hence, this site is clearly dominated by oxygen, as indicated by the chemical composition. This is also consistent with the infrared spectrum, which shows only a weak band for the hydroxyl groups at the *W* site (see above).

6. Discussion

According to the IMA-CNMNC guidelines (Henry *et al*., 2011), the *X* site is dominated by Na, the *Y* site is dominated by Fe^{3+}, the *Z* site is dominated by Al along with Mg (*valency-imposed double-site occupancy*), the *W* site by O^{2-}. Accordingly, this tourmaline is a new species.

In addition, to accommodate the Mg-Al disorder over *Y* and *Z*, we used the procedure recommended by Henry *et al*. (2013), which leads to the formula:

$$\begin{aligned} &{}^{X}(Na_{0.73}Ca_{0.23}\square_{0.04})_{\Sigma 1.00} \\ &{}^{Y}\left(Fe^{3+}{}_{2.40}Fe^{2+}{}_{0.59}Ti^{4+}{}_{0.01}\right)_{\Sigma 3.00} \\ &{}^{Z}\left(Al_{3.36}Mg_{1.69}Fe^{3+}{}_{0.95}\right)_{\Sigma 6.00} \\ &{}^{T}(Si_{5.92}Al_{0.08}O_{18})_{\Sigma 6.00}(BO_3)_3(OH)_3 \\ &{}^{W}\left[O_{0.85}(OH)_{0.15}\right]_{\Sigma 1.00}. \end{aligned} \quad (2)$$

The derived formula is consistent with the end-member formula:

$$NaFe^{3+}_3(Al_4Mg_2)(Si_6O_{18})(BO_3)_3(OH)_3O.$$

Bosiite is a Na-, Fe^{3+}- and Mg-bearing tourmaline, and is isotypic with povondraite and other trigonal (*R*3*m*) members of the tourmaline group such as oxy-dravite (Bosi & Skogby, 2013).Their ideal chemical compositions are given in Table 8. For comparison, chemical analyses and selected physical properties of the valid minerals of the tourmaline supergroup (Henry *et al*., 2011) are given in Table 9. A triangular plot (Fe–Al–Mg) of tourmalines from the bosiite type-locality is shown in Fig. 5 and highlights the main compositional changes.

The refined formula is $^{X}(Na_{0.75}Ca_{0.25})_{\Sigma 1.00}\ ^{Y}(Fe_{2.01}Al_{0.99})_{\Sigma 3.00}\ ^{Z}(Al_{4.15}Fe_{1.85})_{\Sigma 6.00}\ ^{T}(Si_6O_{18})(BO_3)_3\ ^{V}(OH)_3\ ^{W}O$, in reasonable agreement with the optimized formula (1). Slight differences may reflect minor chemical zonation.

The name follows the tourmaline nomenclature recommendations approved by the IMA-CNMNC (Henry *et al*., 2011), which necessitate a new root name for a mineral of the alkali-subgroup 3 with the formula $NaFe^{3+}{}_3(Al_4Mg_2)(Si_6O_{18})(BO_3)_3(OH)_3O$. The new mineral is named after Dr. Ferdinando Bosi (b. 1967), researcher at the University of Rome La Sapienza, Italy, and expert on the crystallography and mineralogy of the tourmaline-supergroup minerals and the spinels.

7. Conclusion

Bosiite, ideally $NaFe^{3+}{}_3(Al_4Mg_2)(Si_6O_{18})(BO_3)_3(OH)_3O$, is related to end-member povondraite, ideally $NaFe^{3+}{}_3(Fe^{3+}{}_4Mg_2)(Si_6O_{18})(BO_3)_3(OH)_3O$, by the substitution $^{Z}Al_4 \rightarrow {}^{Z}Fe^{3+}{}_4$. Further, bosiite is related to oxy-dravite, ideally $Na(Al_2Mg)(Al_5Mg)(Si_6O_{18})(BO_3)_3(OH)_3O$, by

Table 7. Refined site-scattering values (SREF; *epfu*), assigned site-populations (*apfu*) and equivalent site-scattering values (EMPA; *epfu*) for bosiite.

Site	SREF	Site population	EMPA
X	13.3(1)	0.73 Na + 0.23 Ca	12.6
Y	65.1(3)	2.06 Fe + 0.80 Mg + 0.13 Al + 0.01 Ti	65.1
Z	102.0(3)	3.23 Al + 1.88 Fe + 0.89 Mg	101.6

Table 8. Theoretical compositions of bosiite and known Na-rich, Fe^{3+}- and/or Mg-bearing tourmalines (wt%).

	1	2	3	4	5
SiO_2	34.43	31.01	32.91	37.54	37.60
Al_2O_3	19.48	-	27.93	37.16	31.90
B_2O_3	9.97	7.24	9.53	10.87	10.89
FeO	-	-	-	-	-
Fe_2O_3	22.88	48.08	21.87	-	-
MgO	7.70	8.60	-	8.39	12.61
Na_2O	2.96	2.67	2.83	3.23	3.23
H_2O	2.58	2.32	2.47	2.81	3.76
F	-	-	1.73	-	-
X site	Na	Na	Na	Na	Na
Y site	$Fe^{3+}{}_3$	$Fe^{3+}{}_3$	$Fe^{3+}{}_3$	Al_3	Mg_3
Z site	Al_4Mg_2	$Fe^{3+}{}_4Mg_2$	Al_6	Al_4Mg_2	Al_6
B site	B_3	B_3	B_3	B_3	B_3
T site	Si_6	Si_6	Si_6	Si_6	Si_6
V site	$(OH)_3$	$(OH)_3$	$(OH)_3$	$(OH)_3$	$(OH)_3$
W site	O	O	F	O	OH

Notes: 1 – bosiite; 2 – povondraite; 3 – fluor-buergerite; 4 – oxy-dravite (ordered); 5 – dravite.

Table 9. Chemical composition of IMA-approved Na-rich, Fe^{3+}- and/or Mg-bearing tourmalines (wt%).

	1	2	3	4	5
SiO_2	33.44	30.7	33.86	37.01	36.52
TiO_2	0.05	-	0.55	0.14	0.17
B_2O_3	9.82	9.0	10.86	10.76	10.32
Al_2O_3	16.59	1.4	30.79	33.11	33.41
Fe_2O_3	24.98	45.0	17.62	5.00	0.83
FeO	3.97	1.7	1.27	0.19	0.30
MgO	6.41	6.5	0.13	8.56	11.25
Na_2O	2.12	2.1	2.46	2.65	2.34
K_2O	0.01	1.0	0.07	0.10	0.57
CaO	1.21	-	0.69	-	0.42
H_2O	2.67	2.4	0.40	2.65	3.76
F	-	-	1.86	-	0.12
a Å	16.101	16.186	15.873	15.927	15.929
c Å	7.327	7.444	7.187	7.200	7.196
V Å^3	1645.0	1688.9	1566.1	1581.8	1581.3

Notes. 1: bosiite, type locality Darasun mine, Transbaikal Krai, Transbaikalia, Russia (this work). 2: povondraite, San Francisco mine, Villa Tunari, Bolivia (Grice *et al*., 1993). 3: fluor-buergerite, type locality Mexquitic, San Luis Potosí, Mexico (Donnay *et al*., 1966). 4: oxy-dravite, type locality Osarara, Narok district, Kenya (Bosi & Skogby, 2013). 5: dravite, type locality Unterdrauburg, Carinthia (today Dravograd, Slovenia) (Kunitz, 1929; Euromin project, 2007).

the substitutions $^{[6]}Fe^{3+}{}_3 \rightarrow {}^{[6]}Al_3$. It can be distinguished from schorl, povondraite, fluor-buergerite, dravite, oxy-dravite or other dark tourmalines only by accurate determination of the chemical composition, preferably by a combination of single-crystal structure refinement and chemical analysis including Mössbauer spectroscopy. It may also be confused with luinaite-(OH) (IMA 2009–046) and its currently unnamed F-analogue, both representing monoclinically distorted variants (*Cm*) of the tourmaline structure. Relatively large lattice parameters ($a \geq 16.1$, $c \geq 7.3$ Å) and the occurrence in a hydrothermal environment could be preliminary indications for the occurrence of bosiite.

Acknowledgements: We thank V.O. Yapaskurt (Department of Petrology, Lomonosov Moscow State University, Moscow, Russia), S.A. Gorbacheva (IGEM, Russian Academy of Sciences, Moscow, Russia) and A. B. Mironov (Institute of Mineralogy, Ural Division, Russian Academy of Sciences, Miass, Russia) for analytical work. We are grateful to Andreas Wagner (Institut für Mineralogie und Kristallographie, Vienna, Austria) for taking photographs of bosiite. We sincerely thank Frank C. Hawthorne and an anonymous reviewer for constructive comments on this manuscript. This work was supported in part by Austrian Science Fund (FWF) project no. P23012-N19 and no. P26903-N19 to AE, by IGCP 540 and the Russian Foundation for Basic Research (project nos. 09–05–00697a and 09–05–12037ofi–m). The purchase of the electron microscope was financially supported by the Program for the Moscow State University Development.

References

Andreozzi, G.B., Bosi, F., Longo, M. (2008): Linking Mössbauer and structural parameters in elbaite-schorl-dravite tourmalines. *Am. Mineral.*, **93**, 658–666.

Bačik, P., Uher, P., Sykora, M., Lipka, J. (2008): Low-Al tourmalines of the schorl – dravite – povondraite series in redeposited tourmalinites from the Western Carpathians, Slovakia. *Can. Mineral.*, **46**, 1117–1129.

Baksheev, I.A., Chitalin, A.F., Yapaskurt, V.O., Vigasina, M.F., Bryzgalov, I.A., Ustinov, V.I. (2010): Tourmaline mineralization of the Vetka Cu–Mo-porphyry occurrence, Chukotka, Russia. *Moscow Univ. Geol. Bull.*, **65**, 27–39.

Baksheev, I.A., Prokof'ev, V. Yu., Yapaskurt, V.O., Vigasina, M.F., Zorina, L.D., Solov'ev, V.N. (2011): Ferric-iron-rich tourmaline from the Darasun gold deposit, Transbaikalia, Russia. *Can. Mineral.*, **49**, 263–276.

Baksheev, I.A., Prokof'ev, V. Yu., Zaraisky, G.P., Chitalin, A.F., Yapaskurt, V.O., Nikolaev, Y.N., Tikhomirov, P.L., Nagornaya, E.V., Rogacheva, L.I., Gorelikova, N.V., Kononov, O.V. (2012): Tourmaline as a prospecting guide for the porphyry-style deposits. *Eur. J. Mineral.*, **24**, 957–979.

Béziat, D., Bourges, F., Debat, P., Fuchs, Y., Lompo, M., Martin, F., Nikiéma, S., Tollon, F. (1999): The Guibaré and Fété Kolé

gold-bearing tourmaline–quartz veins in the Birimian greenstone belts of Burkina Faso. *Can. Mineral.*, **37**, 575–591.

Bosi, F. (2008): Disordering of Fe^{2+} over octahedrally coordinated sites of tourmaline. *Am. Mineral.*, **93**, 1647–1653.

Bosi, F. & Lucchesi, S. (2004): Crystal chemistry of the schorl-dravite series. *Eur. J. Mineral.*, **16**, 335–344.

—, — (2007): Crystal chemical relationships in the tourmaline group: structural constraints on chemical variability. *Am. Mineral.*, **92**, 1050–1063.

Bosi, F. & Skogby, H. (2013): Oxy-dravite, $Na(Al_2Mg)(Al_5Mg)(Si_6O_{18})(BO_3)_3(OH)_3O$, a new mineral species of the tourmaline supergroup. *Am. Mineral.*, **98**, 1442–1448.

Bosi, F., Lucchesi, S., Reznitskii, L. (2004): Crystal chemistry of the dravite-chromdravite series. *Eur. J. Mineral.*, **16**, 345–352.

Bosi, F., Andreozzi, G.B., Federico, M., Graziani, G., Lucchesi, S. (2005): Crystal chemistry of the elbaite-schorl series. *Am. Mineral.*, **90**, 1784–1792.

Bosi, F., Skogby, H., Hålenius, U., Reznitskii, L. (2013): Crystallographic and spectroscopic characterization of Fe-bearing chromo-alumino-povondraite and its relations with oxy-chromium-dravite and oxy-dravite. *Am. Mineral.*, **98**, 557–1564.

Bosi, F., Skogby, H., Reznitskii, L., Hålenius, U. (2014): Vanadio-oxy-dravite, $NaV_3(Al_4Mg_2)(Si_6O_{18})(BO_3)_3(OH)_3O$, a new mineral species of the tourmaline supergroup. *Am. Mineral.*, **99**, 218–224.

Cavaretta, G. & Puxeddu, M. (1990): Schorl – dravite – ferridravite tourmalines deposited by hydrothermal magmatic fluids during early evolution of Larderello geothermal field, Italy. *Econ. Geol.*, **85**, 1236–1251.

Deer, W.A., Howie, R.A., Zussman, J. (1986): Rock-forming minerals. Vol. 1B: Disilicates and ring silicates. 2nd edn. Longman, Burnt Mill, Harlow.

Donnay, G., Ingamells, C.O., Mason, B. (1966): Buergerite, a new species of tourmaline. *Am. Mineral.*, **51**, 198–199.

Dyar, M.D., Taylor, M.E., Lutz, T.M., Francis, C.A., Guidotti, C.V., Wise, M. (1998): Inclusive chemical characterization of tourmaline: Mössbauer study of Fe valence and site occupancy. *Am. Mineral.*, **83**, 848–864.

Ertl, A. & Tillmanns, E. (2012): The [9]-coordinated *X* site in the crystal structure of tourmaline-group minerals. *Z. Kristallogr.*, **227**, 456–459.

Ertl, A., Pertlik, F., Bernhardt, H.-J. (1997): Investigations on olenite with excess boron from the Koralpe, Styria, Austria. *Österr. Akad. Wiss., Math.-Naturw. Kl., Abt. I, Anzeiger.*, **134**, 3–10.

Ertl, A., Hughes, J.M., Pertlik, F., Foit, F.F, Jr, Wright, S.E., Brandstätter, F., Marler, B. (2002): Polyhedron distortions in tourmaline. *Can. Mineral.*, **40**, 153–162.

Ertl, A., Rossman, G.R., Hughes, J.M., Prowatke, S., Ludwig, T. (2005): Mn-bearing "oxy-rossmanite" with tetrahedrally coordinated Al and B from Austria: structure, chemistry, and infrared and optical spectroscopic study. *Am. Mineral.*, **90**, 481–487.

Ertl, A., Tillmanns, E., Ntaflos, T., Francis, C., Giester, G., Körner, W., Hughes, J.M., Lengauer, C., Prem, M. (2008): Tetrahedrally coordinated boron in Al-rich tourmaline and its relationship to the pressure–temperature conditions of formation. *Eur. J. Mineral.*, **20**, 881–888.

Ertl, A., Marschall, H.R., Giester, G., Henry, D.J., Schertl, H.-P., Ntaflos, T., Luvizotto, G.L., Nasdala, L., Tillmanns, E. (2010): Metamorphic ultra high-pressure tourmalines: structure, chemistry, and correlations to PT conditions. *Am. Mineral.*, **95**, 1–10.

Ertl, A., Giester, G., Ludwig, T., Meyer, H.-P., Rossman, G.R. (2012a): Synthetic B-rich olenite: correlations of single-crystal structural data. *Am. Mineral.*, **97**, 1591–1597.

Ertl, A., Kolitsch, U., Dyar, M.D., Hughes, J.M., Rossman, G.R., Pieczka, A., Henry, D.J., Pezzotta, F., Prowatke, S., Lengauer, C.L., Körner, W., Brandstätter, F., Francis, C.A., Prem, M., Tillmanns, E. (2012b): Limitations of Fe^{2+} and Mn^{2+} site occupancy in tourmaline: evidence from Fe^{2+}- and Mn^{2+}-rich tourmaline. *Am. Mineral.*, **97**, 1402–1416.

Ertl, A., Vereshchagin, O.S., Giester, G., Tillmanns, E., Meyer, H.-P., Ludwig, T., Rozhdestvenskaya, I.V., Frank-Kamenetskaya, O.V. (2015): Structural and chemical investigation of a zoned synthetic Cu-rich tourmaline. *Can. Mineral.*, **53**, 209–220.

Ertl, A., Kolitsch, U., Dyar, M.D., Meyer, H.-P., Henry, D.J., Rossman, G.R., Prem, M., Ludwig, T., Nasdala, L., Lengauer, C.L., Tillmanns, E., Niedermayr, G. (2016): Fluor-schorl, a new member of the tourmaline supergroup, and new data on schorl from the cotype localities. *Eur. J. Mineral.*, **28**, 163–177.

Fischer, R.X. & Tillmanns, E. (1988): The equivalent isotropic displacement factor. *Acta Crystallogr.*, **C44**, 775–776.

Foit, F.F, Jr. (1989): Crystal chemistry of alkali-deficient schorl and tourmaline structural relationships. *Am. Mineral.*, **74**, 422–431.

Foit, F.F, Jr & Rosenberg, P.E. (1979): The structure of vanadium-bearing tourmaline and its implications regarding tourmaline solid solutions. *Am. Mineral.*, **64**, 788–798.

Fuchs, Y., Lagache, M., Linares, J. (1998): Fe-tourmaline synthesis under different T and $fO2$ conditions. *Am. Mineral.*, **83**, 525–534.

Grice, J.B. & Ercit, S.T. (1993): Ordering of Fe and Mg in the tourmaline crystal structure: the correct formula. *Neues Jahrb. Mineral. Abh.*, **165**, 245–266.

Grice, J.D., Ercit, T.S., Hawthorne, F.C. (1993): Povondraite, a redefinition of the tourmaline ferridravite. *Am. Mineral.*, **78**, 433–436.

Hawthorne, F.C. (1996): Structural mechanisms for light-element variations in tourmaline. *Can. Mineral.*, **34**, 123–132.

— (2002): Bond-valence constraints on the chemical composition of tourmaline. *Can. Mineral.*, **40**, 789–797.

Hawthorne, F.C., MacDonald, D.J., Burns, P.C. (1993): Reassignment of cation site-occupancies in tourmaline: Al-Mg disorder in the crystal structure of dravite. *Am. Mineral.*, **78**, 265–270.

Henry, D.J. & Dutrow, B. (1996): Metamorphic tourmaline and its petrologic applications. *in* "Boron: Mineralogy, Petrology and Geochemistry", E.S. Grew & L.M. Anovitz, eds. *Rev. Mineral.*, **33**, 503–557.

Henry, D.J., Kirkland, B.L., Kirkland, D.W. (1999): Sector-zoned tourmaline from the cap rock of a salt dome. *Eur. J. Mineral.*, **11**, 263–280.

Henry, D.J., Sun, H., Slack, J.F., Dutrow, B.L. (2008): Tourmaline in meta-evaporites and highly magnesian rocks: perspectives from Namibian tourmalinites. *Eur. J. Mineral.*, **20**, 889–904.

Henry, D., Novák, M., Hawthorne, F.C., Ertl, A., Dutrow, B.L., Uher, P., Pezzotta, F. (2011): Nomenclature of the tourmaline-supergroup minerals. *Am. Mineral.*, **96**, 895–913.

Henry, D.J., Novák, M., Hawthorne, F.C., Ertl, A., Dutrow, B., Uher, P., Pezzotta, F. (2013): *Erratum*. Nomenclature of the tourmaline supergroup minerals. *Am. Mineral.*, **98**, 524.

Hughes, J.M., Ertl, A., Dyar, M.D., Grew, E., Wiedenbeck, M., Brandstätter, F. (2004): Structural and chemical response to

varying $^{[4]}$B content in zoned Fe-bearing olenite from Koralpe, Austria. *Am. Mineral.*, **89**, 447–454.

Hughes, J.M., Rakovan, J., Ertl, A., Rossman, G.R., Baksheev, I., Bernhardt, H.-J., (2011): Dissymetrization in tourmaline: The atomic arrangement of sectorally zoned triclinic Ni-bearing dravite. *Can. Mineral.*, **49**, 29–40.

Jarosewich, E.J., Nelen, J.A., Norberg, J.A. (1980): Reference samples for electron microprobe analysis. *Geostandards Newslett.*, **4**, 43–47.

Kunitz, W. (1929): Die Mischungsreihen in der Turmalingruppe und die genetischen Beziehungen zwischen Turmaline und Glimmern. *Chemie der Erde*, **4**, 208–251.

Lynch, G. & Ortega, J. (1997): Hydrothermal alteration and tourmaline–albite equilibria at the Coxheath porphyry Cu–Mo–Au deposit, Nova Scotia. *Can. Mineral.*, **35**, 79–94.

MacDonald, D.J. & Hawthorne, F.C. (1995): The crystal chemistry of Si ↔ Al substitution in tourmaline. *Can. Mineral.*, **33**, 849–858.

Povondra, P. & Čech, A. (1976): A method for the chemical analysis of tourmaline. *Acta U. Carol. Geol.*, **1976**, 209–218.

Reznitskii, L., Clark, C.M., Hawthorne, F.C., Grice, J.D., Skogby, H., Hålenius, U., Bosi, F. (2014): Chromo-alumino-povondraite, $NaCr_3(Al_4Mg_2)(Si_6O_{18})(BO_3)_3(OH)_3O$, a new mineral species of the tourmaline supergroup. *Am. Mineral.*, **99**, 1767–1773.

Sheldrick, G.M. (1998): SHELXL97, Release 97–2. Program for crystal structure refinement. University of Göttingen, Göttingen, Germany.

Taylor, M.C., Cooper, M.A., Hawthorne, F.C. (1995): Local charge-compensation in hydroxyl-deficient uvite. *Can. Mineral.*, **33**, 1215–1221.

The Euromin project. (2007): Dravite. http://euromin.w3sites.net/mineraux/DRAVITE.html

Wright, S.E., Foley, J.A., Hughes, J.M. (2000): Optimization of site-occupancies in minerals using quadratic programming. *Am. Mineral.*, **85**, 524–531.

Žáček, V., Petrov, A., Hyršl, J. (1998): Chemistry and origin of povondraite-bearing rocks from Alto Chapare, Cochabamba, Bolivia. *J. Czech Geol. Soc.*, **43**, 59–67.

Received 2 November 2015
Modified version received 4 February 2016
Accepted 14 March 2016